XX Polish Fluid Mechanics Conference,
Gliwice, 17-20 September 2012

EFFECT OF INFLOW VARIATIONS ON COMPRESSOR SECONDARY FLOW BEHAVIOR

Pingping Chen [1,2], Karsten Liesner[1], Robert Meyer[1], Weiyang Qiao[2]
1 DLR Institute of Propulsion Technology, 10623 Berlin, Germany;
2 Northwestern Polytechnical University, 710072 Xi'an, China
E-mail: pingping.chen@dlr.de

Abstract

In this paper numerical and experimental investigations have been presented on a high-speed compressor cascade (consisting of NACA 65-K48 profiles) with inflow variations (including inlet boundary layer thickness and inflow turbulence intensity variations). The effects of inlet boundary layer thickness and inflow turbulent intensity on the compressor secondary flow behavior are discussed. In the experiment, data were obtained using robust measurement techniques with total pressure and angle probe rake for the loss and flow turning and flow visualization techniques with oil-streak patterns on the stator vanes surfaces. In the numerical simulations, the 3D RANS flow solver TRACE is used with fully turbulent setting to calculate the inflow variations' influences. The results of numerical simulations and experiment show that the inlet boundary layer thickness have great influences on the secondary flow behavior, especially the corner separation/vortex; the inlet turbulence however affects it less; but both of these inlet variations contribute to different exit flow loss distributions.

Key words: inlet boundary layer thickness; inflow turbulent intensity; high-speed compressor cascade; secondary flow behavior, TRACE

INTRODUCTION

With regards to the compressor-components of advanced gas turbine, the continual development towards an increased overall pressure ratio and higher compressor efficiency leads to higher loadings and lower aspect ratios in the modern axial flow compressor, whereas this also causes much more complex internal flow. Consequently, this leads to more complex flow pattern, higher losses and a more complicated trigger mechanism for the flow instability. In order to achieve a better compressor performance, the instability mechanism needs to be well studied. However, for the modern compressor, the flow efficiency is diffused over the 60-80% of the span, and the end wall and corner regions are thus the keys to aerodynamic blockage, loss production, and compressor instability. So the unstable flow in the corner region, which is referred to in many research works, should be treated theoretically and completely[1、2].

In Horlock and Denton's work [3], though the classical secondary flow in compressors is not as strong as in turbines because of the low blade turning, the thick end wall boundary layers are still apt to separate in the corner region between the suction surface and the end wall. Moreover, the secondary flows have great roles on the development of this separation, which means that the secondary flows can intensify it in fact.

The study of secondary flow is of keen interest for researchers to achieve a better compressor performance and to avoid such instability problems. Owing to the viscous flow

and the non-uniform inflow, the secondary flow becomes substantial for the critical performance demands. The mechanism of secondary flow is firstly well described by Horlock et al [4]. The end wall boundary layer has a lower velocity than the freestream, but experiences the same cross-stream pressure gradient as the freestream. Thus, the streamline radius of curvature near the end wall is smaller than in the freestream, resulting in cross-passage motion and the accumulation of low stagnation pressure fluid near suction surface hub corner. If the blade loading is high enough, this fluid will not be able to produce the blade passage pressure rise and hub-corner stall will commence, increasing the blockage and thus the passage loss, lowering the pressure rise capability of blade row, and increasing the entropy rise when the flow interacting with downstream.

So the mechanism of secondary flow should be investigated firstly as a reference of the mechanism of flow instability and the further research of related flow control techniques. For the viscous flow, the inlet flow condition influences the internal flow a lot. However, many substantial numerical and experimental works [1、2] have been done on the cascade performance with clean inlet and nearly uniform axial velocity profile, though in Smith's study(cited in reference [5]), the boundary layer thickness on the hub and casing is increased while the flow goes through the blade row of a multi-stage axial compressor. Then, its conclusion has been applied to many research works of multi-stage turbomachinery without too much consideration of the inlet boundary layer thickness. In 1980s, Wagner et al.[6、7] studied the effect of inlet boundary layer thickness on the internal flow in a turbomachinery. In 2006, Feng et al. [8] numerically investigated the influence of inlet boundary layer on flow field performance of 2D compressor bowed stator vane. In 2010 ASME conference, Minsuk Choi et al. [5] studied the effects of the inlet boundary layer thickness on the internal flow and the loss characteristics in a low-speed axial compressor with three-dimensional computation, and then found different characteristics of hub-corner stall and the tip leakage flow with thin and thick inlet boundary layers at the design and near stall conditions.

For the boundary layer flow near the blade suction surface, although the main stream can be set to fully turbulent, the boundary layer maybe either laminar or turbulent, and the transition mostly happens due to the high level of freestream turbulence intensity. In addition, the performance of compressors can be highly affected by transition because this phenomenon may be crucial to generating large separation regions which will have a considerable impact on flow losses [9-11]. So the inlet turbulence intensity, which will lead to different flow patterns in the boundary layer regions near the blade surface, needs to be considered in this study.

On the other side, the laminar boundary layer separation and transition is a considerable problem on the profile of turbomachinery within the viscous inner-flow of aero engine [12]. One of the critical parameters is the inflow turbulent intensity, which will not only affect the boundary layer flow style but also influence the transition onset. So this parameter will also affect flow patterns in the boundary layer on the blade surface. In Luo's dissertation [12], the effect of inflow turbulence was studied on the boundary layer separation and transition in a turbine cascade and was found to influence the disturbance of the boundary shear layer sensitively. Higher inflow turbulence will not only improve the initial average disturbance level, and accelerate the disturbance growth rate, but also reduce its amplitude. In our investigation, since the target is to well reveal the secondary flow mechanism with different inlet boundary layer thickness and the secondary flow, especially the onset of corner separation, will be affected a lot by the inflow turbulent intensity, as a result, its influence should be examined carefully firstly.

In this paper, to capture the internal flow well, numerical and experimental methods are carried out with inflow variations in a high-speed compressor cascade (consisting of NACA-65 K48 profiles). In the present investigation, the influences of inlet boundary layer thickness

and the inlet turbulence are investigated mainly by numerical simulations which are validated by our experiment. It has been observed that the inlet boundary layer thickness has a great influence on the secondary flow behavior, especially the corner separation/vortex; the inlet turbulence however affects it less; but both of these inlet variations can contribute to different exit flow loss distributions.

CASCADE CONFIGURATION

In our numerical investigation, the linear compressor cascade configuration is a high-speed compressor cascade consisting of 5 blades with a NACA-65 K48 profile [13]. The blade profile and the general design parameters and test conditions at the aerodynamic design point are shown in Table 1.

The design Mach number at the inlet is Ma_1=0.67, with which the design Reynolds number is correspondingly 560 000 based on the blade chord of 40 mm. The aspect ratio is s/c =1, which will emphasize the secondary flow behavior much more clearly. Otherwise, this value is a typical one for the rear stages of high-pressure compressor. At the design point the inflow angle is α_1=42° and the turning angle is 48°. The stagger angle is 22.5°.

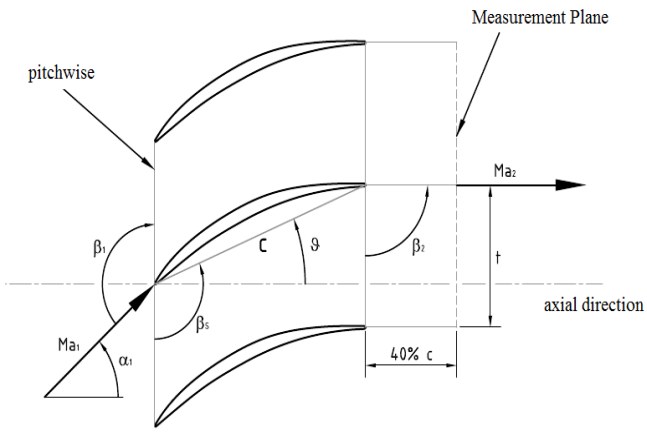

Fig. 1 Cascade configuration

Tab. 1 Cascade design parameters and test conditions

Parameter	Variable	Value	Unit
No. of blades	—	5	—
Chord length	c	40	mm
Blade span	h	40	mm
Blade pitch	t	22	mm
Aspect ratio	h/c	1	[-]
Pitch to chord	t/c	0.55	[-]
Stagger angle	α_s	22.5	degree
Inflow angle	α_1	42	degree
Inlet Mach number	Ma_1	0.67	[-]
Inlet Reynolds number	Re_1	560 000	[-]

NUMERICAL APPROACH

For the numerical simulations, the 3D-RANS flow solver TRACE [14] is used including a k-ω turbulence model with fully turbulent setting. The utilized meshes are generated with G3DMESH [15]. Both of these codes are developed by the German Aerospace Center (DLR) in Cologne especially for turbomachinery applications.

Turbulence Model

In order to well reveal the effects of inlet boundary layer thickness and inlet turbulence intensity on the flow mechanism of secondary flow, the Menter k-ω two-equation turbulence model with fully turbulent setting is carried out in the steady numerical simulations. Kato-Launder-Modification is used to modify the turbulence model's production terms [14]. In our study, the Mach number of the flow field will be fixed at approximately 0.67, so taking compression effects into consideration, a correction for the compressible mixing layer (dilatation dissipation) is used in the calculation. This addition corrects the prediction of mixing layer growth in the compressible flow, which is not properly predicted by standard formulations starting at M > approx. 0.5. This correction is achieved by modifying the destruction terms' closure coefficients.

Grid System

According to the flow solver and turbulence model, the mesh is structured with blocks and about 25 grid nodes are applied to resolve the flows in the blade boundary layer, which ensuring the dimensionless wall distance of $y^+ < 1$.

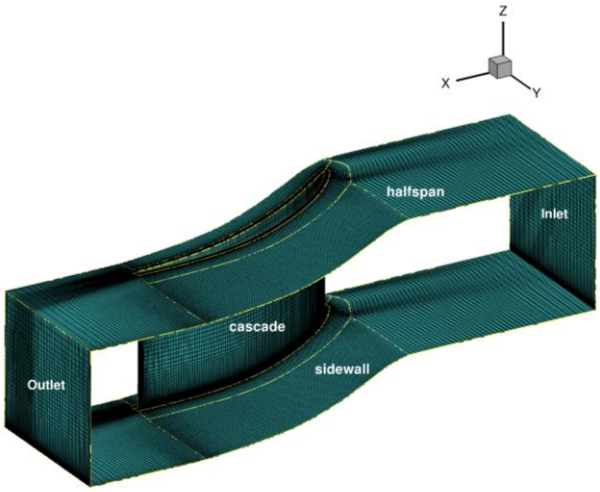

Fig. 2 computational domain and grids

Due to the symmetry boundary condition setting demonstrated below, only half of the span is considered in the steady simulation. The computational domain is chosen from 33mm ahead of the blade leading edge to 18mm behind the blade trailing edge. A multiplied O-C-H type mesh is used in the calculation, and the details are listed in the following table.

Tab. 2 Grids information of half span of the Cascade

Blocks' name	Mesh type	nodes	I-index	J-index	K-index
Blase BL_PS	O	246 525	173	25	57
Blade BL_SS	O	246 525	173	25	57
Connnecting section_PS	C	119 301	161	13	57
Connnecting section_SS	C	119 301	161	13	57
Passage	H	313 215	157	35	57
Inlet	H	161 253	41	69	57
Outlet	H	226 233	49	81	57
Total	-	1 432 353	-	-	-

Boundary Conditions

Inflow and Outflow: Based on a characteristic analysis of the linearized Euler equations, the non-reflecting boundary conditions are defined at the domain inlet and outlet. Especially, to determine the inlet flow quantities, the total pressure, total temperature, inflow angle, turbulent intensity, turbulent length scale and inflow Mach number are given with flux average as an inlet input file; meanwhile, the static back pressure, with radial equilibrium located at the midspan under mass average, is defined as the outlet boundary condition.

For our focus on the effect of inflow condition variations, the inlet boundary thickness and inflow turbulent intensity are varied as follows:

1) Inlet boundary layer thickness variation

In this section, the distribution of inlet total pressure is varied to change the inlet boundary layer thickness from 1mm to 5mm. Here, 3.15mm is the design inlet boundary layer thickness.

When studying on the effect of inlet boundary layer thickness on the secondary flow mechanism, the inflow turbulent intensity is fixed at T_u=2%

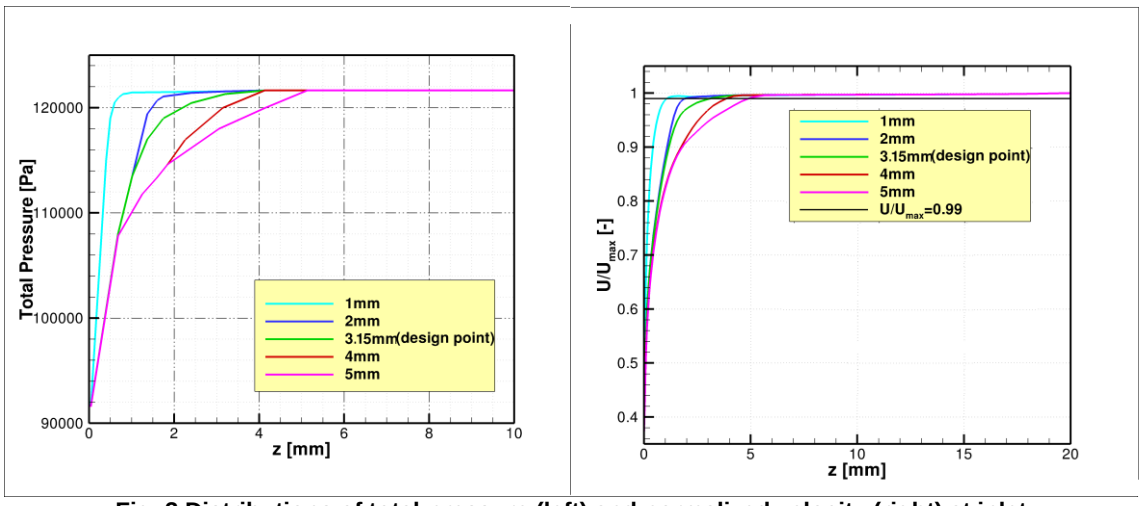

Fig. 3 Distributions of total-pressure (left) and normalized velocity (right) at inlet

2) Inflow turbulent intensity

The inflow turbulent intensity will be varied from 0.5% to 4% as the second focus in this paper. Similarly, when simulating the inflow turbulent intensity's influence on the secondary flow behavior, the inlet boundary layer thickness is fixed at 3.15mm, as required.

Tab. 3 inflow turbulent intensity

No. of cases	T_u
1	0.5%
2	1%
3	2%
4	4%

Blade and sidewall: In the viscous flow simulation, the adiabatic wall setting is used as the conditions of the blade and sidewall. The adiabatic wall is a kind of wall without flow on the wall surface and without heat transferring under a constant wall temperature Tw, which is realized by proper setting of the density in the ghost cells, while the pressure is mirrored as in the adiabatic case.

Symmetry Condition: Mirror. At symmetry boundaries, all flow should disappear, neither mass nor energy exchange can be given. This can be realized by setting the ghost cell values with the interior cell values mirrored at the boundary face. So in our simulation, a symmetry plane can be defined at halfspan of the linear cascade.

Periodic Boundary: In linear cases, the values of ghost cell are taken from the shadow block at the periodic boundaries. So, all the flow values of passage on one side will be copied to the other side.

DATA EVALUATION

Flow loss

Theoretically, the flow loss can be separated as three parts: the profile loss, the endwall loss and the secondary flow loss [16].

$$\varsigma_{General} = \varsigma_{Profile} + \varsigma_{sidewall} + \varsigma_{secondary}$$

Here, the general flow loss is the total pressure loss, the sidewall loss can be calculated by the inlet boundary layer loss, and the profile loss is due to the viscous flow loss around the blade, which can be obtained from the midspan total pressure loss at the exit (the Measurement Plane).

$$\varsigma_{General} = \varsigma_{TP}$$

$$\varsigma_{sidewall} = \varsigma_{BL}$$

So, the secondary flow loss can be computed as a result.

$$\varsigma_{secondary} = \varsigma_{General} - \varsigma_{Profile} - \varsigma_{sidewall}$$

$$= \varsigma_{TP} - \varsigma_{Profile} - \varsigma_{BL}$$

Where, the total pressure loss can be computed by

$$\varsigma_{TP} = \frac{P_t(x,y,z) - P_{t1}}{P_{t1} - P_{s1}}$$

Additionally, a mass flow weighted average method is used in all calculations by the integration perform of Tecplot to get the reasonable data for analysis.

Static pressure rise

To obtain an improved compressor performance, the static pressure rise is a critical parameter for the analysis, which is defined as $(\Delta p/q_1) = (p_2 - p_1)/q_1$.

Wall shear stress

Due to the slip-wall condition, the flow has no velocity normal to the wall. So the wall shear stress is defined as the following:

$$\tau_w = \mu\sqrt{\left(\frac{\partial U}{\partial x}\right)^2 + \left(\frac{\partial V}{\partial y}\right)^2 + \left(\frac{\partial W}{\partial z}\right)^2}$$

Flow turning angle (or the outflow angle)

Flow turning angle can be one of the representatives for the performance of a compressor stage. So in our study, the flow angle should be investigated. In this part, the inlet flow angle is fixed at $\alpha_1 = 42^o$, so the flow turning angle is only associated with the outflow angle. Simply, we use outflow angle measured to analyze the blade loading.

$$\Delta\alpha = \alpha_1 - \alpha_2 \quad (\text{or } \Delta\beta = \beta_1 - \beta_2,\ \beta_x = \alpha_x + 90)$$

RESULTS AND ANALYSIS

Base flow validated by experimental results

With k-ω turbulence model, all cases in this part are calculated with fully turbulent setting. In TRACE, only half span of the cascade is computed. With the symmetry boundary condition at the half-span, we can analyze the whole span in a mirror way. The operations are carried out with turbulent intensity of 2% and a designed inlet boundary layer thickness of 3.15mm, at the inlet Mach number of 0.67, Reynolds number of 560 000, inflow angle of 42°.

In the experimental validation part of this investigation, the High Speed Wind Tunnel [1] of the German Aerospace Center (DLR) is used for validation of the calculations. Its robust measurement techniques allow for a qualified statement of flow quantities and topology. The tripwires with a height of 50mu are applied and located at the 10% chord near the blade leading edge on both sides of the cascade. For the loss and flow turning investigation, a total pressure and angle probe rake is used in the measurement plane, 0.4 times the chord length

downstream of the trailing edge. For the flow topology comparison, flow visualization techniques with oil-streak patterns are used on the stator vanes surfaces.

The general performances of base flow are listed in Table 4 with experimental validation. The difference of the performance values of simulation and experiment are really small, especially static pressure rise and the boundary layer flow loss induced by the viscous wall and secondary loss. With the analysis of the differences of total pressure loss (0.0158) and profile loss (0.0155) between simulation and experiment, since the difference value of 0.0155 is far greater than 0.0003, but quite close to 0.0158, so it can be obtained that, the difference of profile loss contribute the most on the total pressure loss difference. So the simulation of viscous wall boundary layer flow and the secondary flow can be applied for the analysis of the flow mechanism.

Tab. 4 evaluation of general performance for base flow

	experiment	simulation	Δ
ς_{TP}	0.1	0.1158	0.0158
$\varsigma_{Profile}$	0.047	0.0625	0.0155
$\varsigma_{wall+secondary}$	0.053	0.0533	0.0003
$(\Delta p/q_1)$	0.371	0.412	0.041
β_2 [°]	99.7	97.57	-2.13

The contour of local total pressure loss coefficient on the exit plane and the span-wise distribution of pitch-averaged outlet flow angle and total pressure loss coefficient are shown in figure 4. The related vortex structures are shown in figure 5.

In figure 4(a) and 4(b), basically, though the outlet flow angle distributions between experiment and simulation do not agree very well, but the total pressure loss coefficient distribution of secondary flow part in simulation is consistent quite well with the experiment. The profile loss and the boundary layer loss are overestimated by the flow solver in the simulation, which can be found in figure 4(c). In figure 4(c), the black line in the middle of total pressure loss contour divides the figure into two parts: the left is the result of simulation, and the right one is experiment result. At the mid-span, since no secondary flow effect can be observed in figure 5, the losses are mainly caused by the profile due to the viscous boundary layer flow near the surface of the blade. So the profile loss in the left side can also be found greater than in the right side, which is consistent with the conclusion from figure 4(b). The other discrepancy between experiment and the simulation is the region of the highest losses. In the experiment they are located near the mid-span (from 50% to 70% span) and the wall (> 95% span), while in the simulation, from the wall to nearly 38% span, there is a high loss region (flow loss is over 0.3.).

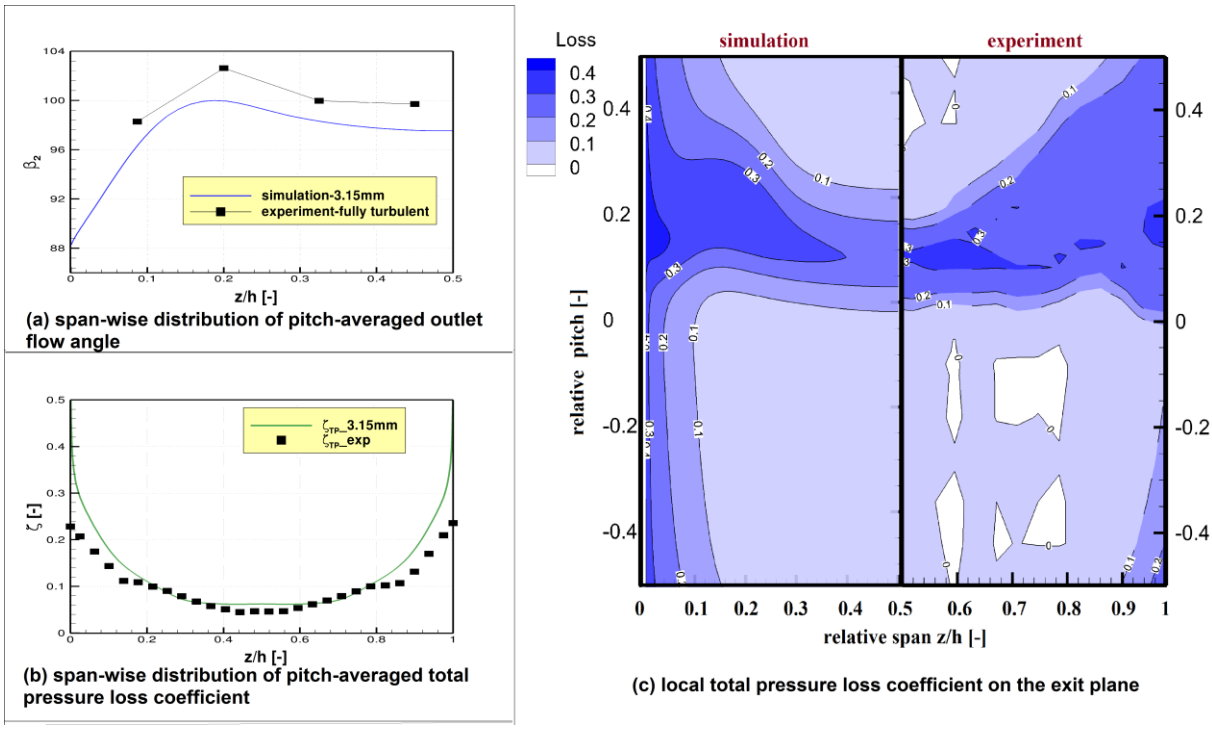

Fig. 4 Evaluation of base flow performance with experimental validation

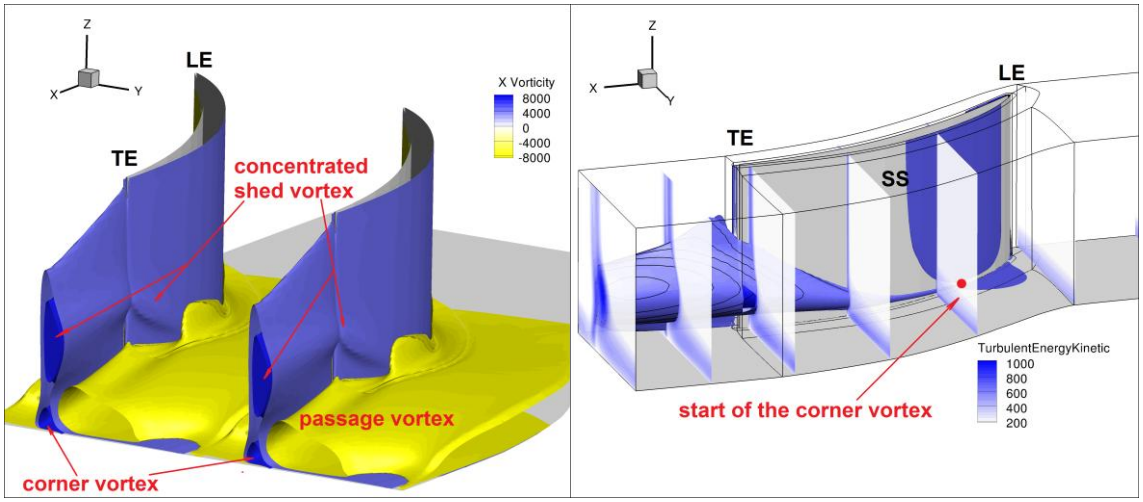

(a)Vortex stuctures with axial vorticity iso-surfacse (b) Secondary flow behavior with TKE iso-surface
Fig. 5 Visualization of the vortex structures (base flow)

In figure 5(a), the isosurfaces are color-coded by the local axial voticity, and the view is from the downstream into the cascade and for the half-span only. The vortexes rotating counter-clockwise are in dark blue and the clockwise vortexes are in yellow. With the help of figure 5(a), three known vortex structures are pointed out as the passage vortex, the corner vortex and the concentrated shed vortex. Related to the λ_2-criterion, there is a small branch observed on the blade suction side at about 20% span, which is the start part of the concentrated shed vortex. Nearby, part of passage vortex is rolled up while some parts are down. In this case, the flow throughout the passage is mainly dominated by the passage vortex and concentrated shed vortex.

The isosurfaces and contours in figure 5(b) are colored by the local turbulent kinetic energy. The concentrated shed vortex can be observed from approximately 30% chord to the exit plane. The branch from around 30% chord (the red spot) can be obviously seen in this

figure. This is the start of both the concentrated shed vortex and the corner vortex which has much lower velocity gradients than the mainstream. When it develops to nearly 60% chord, the corner vortex begins to grow along span-wise and pitch-wise severely. Combined with figure 4(c), it can be concluded that the concentrated shed vortex is the main contribution to the total pressure loss coefficient.

Generally, the agreement is still very good and the numerical methods seem to be able to capture the detailed secondary flow structure and the flow loss.

Effect of Inlet boundary layer thickness

The operations in this section are defined to vary the inlet boundary layer thickness at same condition as the base flow with the inflow turbulent intensity of 2%. Here, the compressor performance and the detailed flow mechanism will be shown and analyzed.

1) General compressor performance

For the viscous flow in a cascade, the increased inlet boundary layer thickness means an increased region of low momentum near-wall, which will firstly and obviously leads to an augmented inlet Boundary layer loss shown in Table 5. The normalized values are used here to evaluate the cascade performance.

Tab. 5 General performance of NACA-65 K48

	δ_{99}=1mm	δ_{99}=2mm	$\delta_{99,design}$=3.15mm	δ_{99}=4mm	δ_{99}=5mm
ς_{TP}	0.856	0.970	1.000	1.094	1.133
$\varsigma_{Profile}$	0.991	0.998	1.000	1.016	1.008
$\varsigma_{wall+secondary}$	0.696	0.937	1.000	1.185	1.280
$(\Delta p/q_1)$	1.023	1.009	1.000	0.974	0.945
β_2 [°]	0.997	0.999	1.000	1.003	1.004

When the viscous flow moves further in the passage, it will meet with the profile. Then due to the adiabatic wall defined on the blade wall, the separations or the low-velocity flow near blade surface will cause an augmented profile loss with the increased inlet boundary layer thickness. From the values in Table 5, the profile loss and outlet flow angle change much smaller than the other parameters. So with the definition of near-wall boundary layer loss and secondary flow loss, the values can be calculated simply as shown in the above table, and it is found that normally as the inlet boundary layer thickness increasing, the total pressure loss, the profile loss, the near-wall boundary layer loss and the secondary loss will be augmented, while the static pressure rise is decreased, as shown in figure 6.

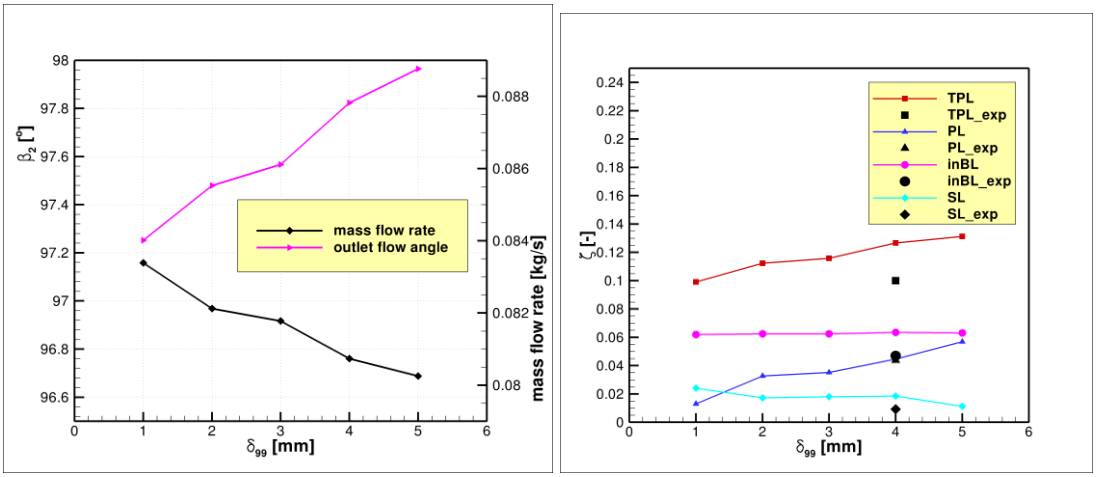

Fig. 6 Gerneral performance of NACA-65 K48 with inlet boundary layer thichness variations (left: mass flow rate and outlet flow angle, right: flow loss)

2) Total pressure flow loss

The span-wise distributions of flow loss and outlet flow angle are shown in Figure 7, compared with the experiment data. Here the profile loss of experiment is much lower than all the simulations.

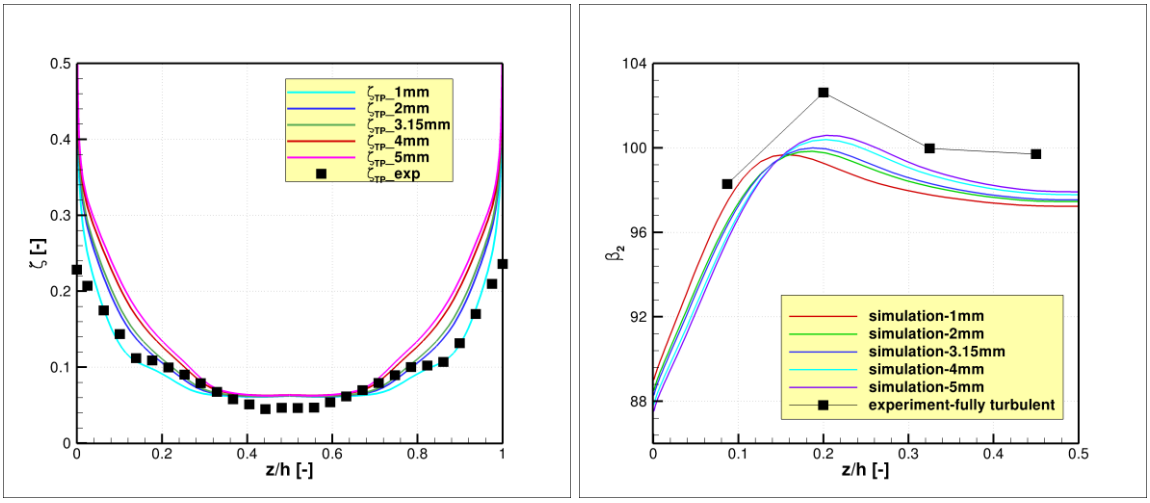

Fig. 7 Flow loss (left) and Outlet flow angle (right)

The total-pressure loss from experiment with tripwires located at the 10% chord on both sides of the cascade is much lower than the simulations. But it agrees quite well with the simulation of δ_{99}=3.16mm at the 16%-36%span. As defined in our former reports, this is the main region dominating the secondary flow loss. So the results here are similar between the simulation and the experiment.

Combined with table 5, the development of outflow angle β_2 at mid-span is much smaller with the increasing boundary layer thickness, but follows the same tendency as the total-pressure loss.

However, with regard to the span-wise distribution of outflow angle, it reveals a quite different behavior in figure 7. The thickness of the boundary layer by 1mm leads is a slight deterioration of the deflection in the region z / h> 0.15, while a minimal improvement can be recognized below z/h = 0.15. Equivalent behaviors are also obtained by the other inlet boundary layer thicknesses. But, in the middle section of the span there is an improvement by much bigger inlet boundary layer thickness, while with respect to the regions about z/h <0.15, deterioration occurs.

3) Exit flow loss

Figure 8 is the total-pressure loss contours at passage exit. With different inlet boundary layer thicknesses, the contours appear changeable. When the inlet boundary layer thickness increases, the high loss area is consequently augmented; with the improved inlet boundary layer flow loss observed from figure 8(a) to 8(e), the total pressure loss distribution are stated various, with location of the high loss area ($\zeta > 0.3$) changed.

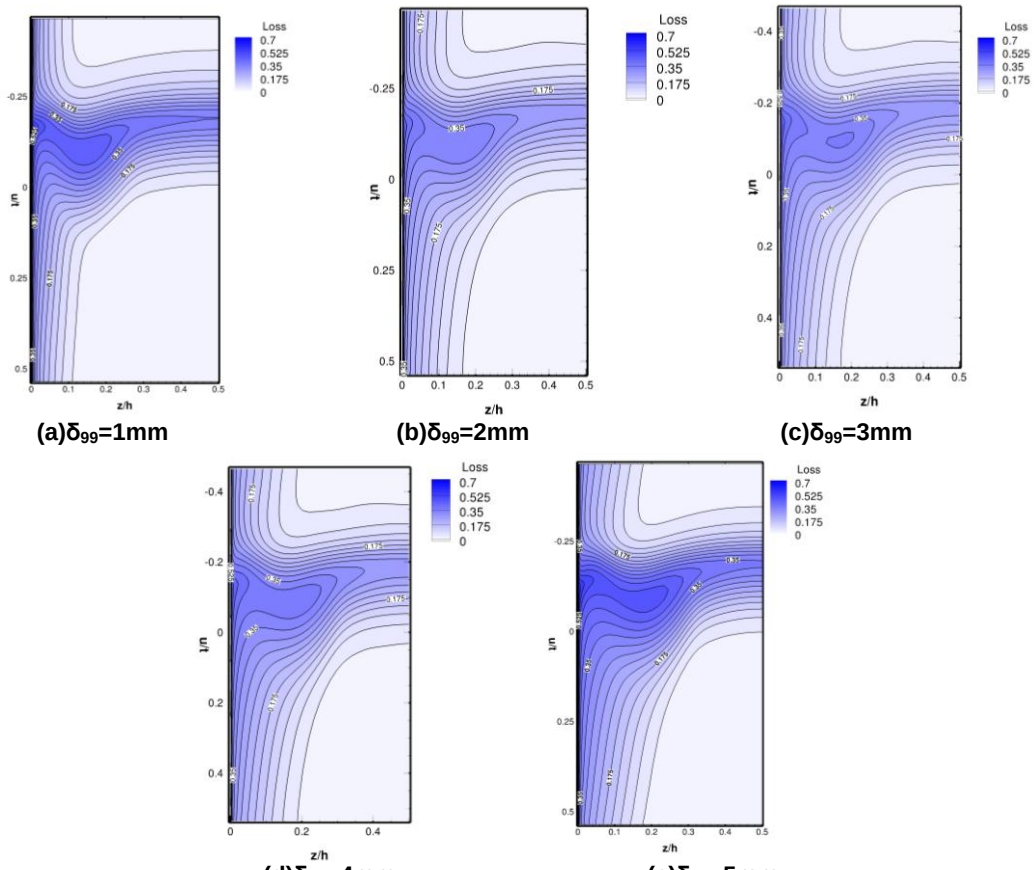

(a)δ_{99}=1mm (b)δ_{99}=2mm (c)δ_{99}=3mm

(d)δ_{99}=4mm (e)δ_{99}=5mm

Fig. 8 Total pressure loss at exit

4) Limiting streamlines and wall shear stress (suction side)

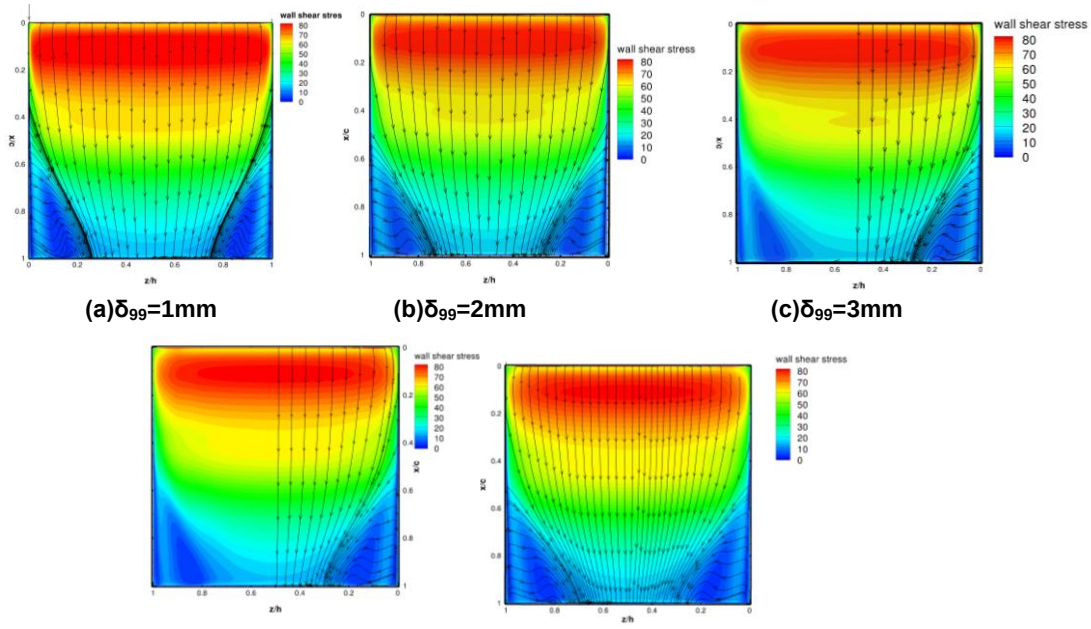

(a)δ_{99}=1mm (b)δ_{99}=2mm (c)δ_{99}=3mm

(d)δ_{99}=4mm (e)δ_{99}=5mm

Fig. 9 Suction side limiting streamlines and wall shear stress

Figure 9 shows the suction side wall streamlines and wall shear stress of the simulations with different inlet boundary layer thicknesses. The influence of inlet boundary layer

thickness on the corner separation/vortex is significant, not only on the scale and intensity of the corner separation area, but also on the wall shear stress distributions on the suction surface. With an increased inlet boundary layer, the region and intensity of high wall shear stress are decreased; meanwhile, the corner separation is augmented along span-wise and axial directions.

5) Iso-surface of axial vorticity

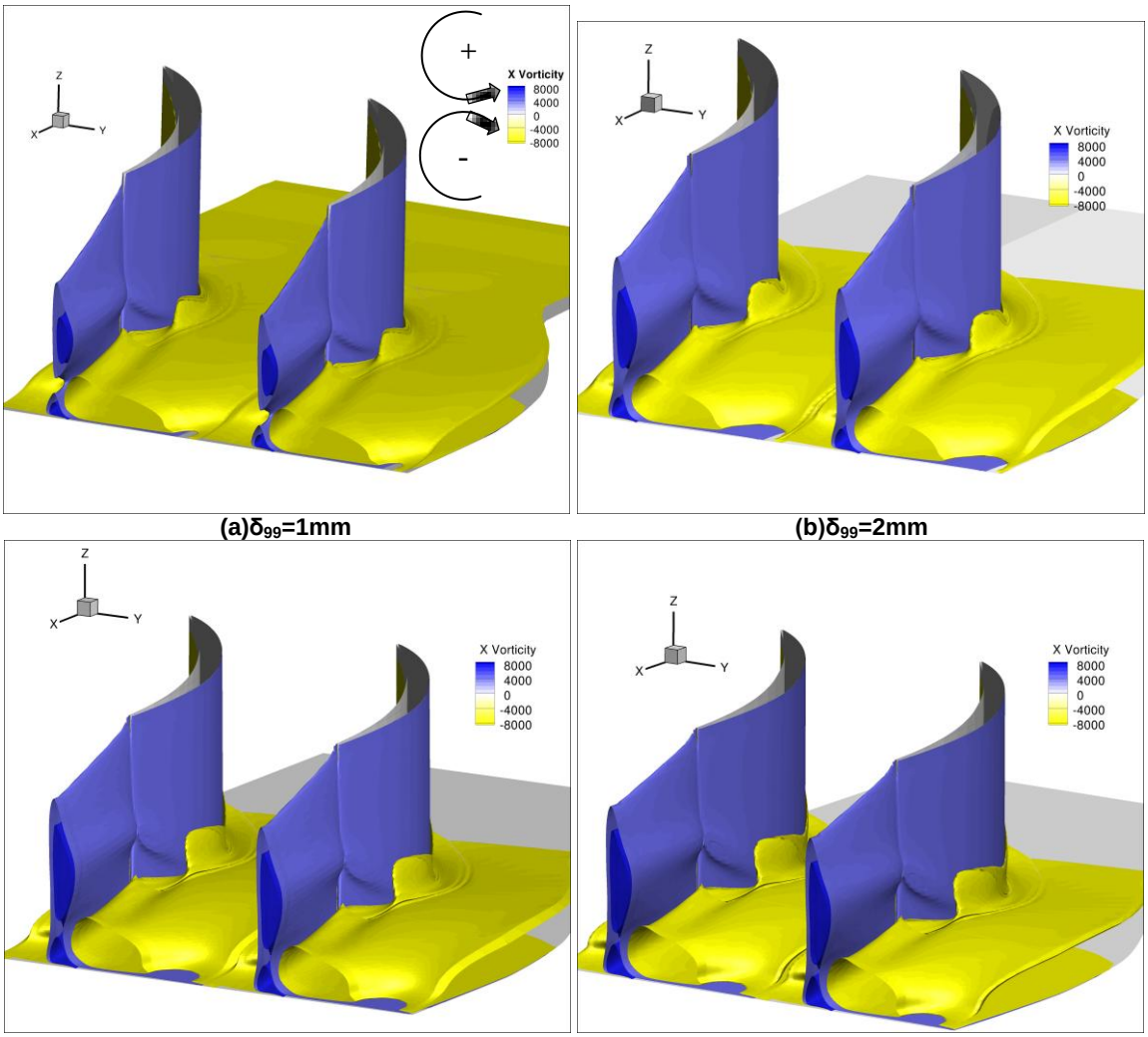

(a)δ_{99}=1mm **(b)δ_{99}=2mm**

(c)δ_{99}=4mm **(d)δ_{99}=5mm**

Fig. 10 Iso-surface of X Vorticity

The horseshoe vortex on the suction side is near the corner region of the profile and the sidewall, but the pressure-side branch induced by the pressure gradient between the neighboring two cascades tends to develop in the passage and then becomes part of the passage vortex. So here, in figure 10, the passage vortex is opposite to the corner vortex and the concentrated shed vortex starting at the blade suction surface. The inlet boundary layer thickness not only affects the development of horseshoe vortex, but also improves the concentrated shed vortex and the corner vortex, which can be observed clearly from figure 13 and 5(a). The inlet boundary layer thickness influences not only the intensity of the concentrated shed vortex, but also the span-wise location of the vortex core of concentrated shed vortex, which is higher with the increased inlet boundary layer thickness..

Effect of Inflow Turbulent Intensity

The operations in this section are defined to vary the inflow turbulent intensity at same condition as the base flow with the designed inlet boundary layer thickness.

1) General cascade performance

As what introduced above, the inflow turbulent intensity will affect the disturbance level of boundary shear layer flow. So its effect on our cascade performance is shown in Table 6 with the normalized values based on the design parameters.

Tab. 6 General performance with different inflow turbulence

	Case 1	Case 2	Case 3	Case 4
	T_u=0.5%	T_u=1.0%	T_u=2%(design)	T_u=4.0%
ς_{TP}	1.001	0.989	1.000	1.085
$\varsigma_{Profile}$	0.957	0.956	1.000	1.162
$\varsigma_{wall+secondary}$	1.042	1.021	1.000	1.012
$(\Delta p/q_1)$	1.001	1.033	1.000	1.015
β_2 [°]	0.999	0.997	1.000	0.999

The hollow tendency can be found as the flow loss behaviors with different inflow turbulence from table 5. The inflow turbulent intensity has a noticeable influence on the profile loss and little effect on the total pressure loss. Hence, the design case of T_u=2% has a better performance with the lowest value of static pressure rise and loss of near-wall boundary layer flow and secondary flow and the best outlet flow angle.

2) Distributions of outlet flow angle and flow loss and contours of exit flow loss

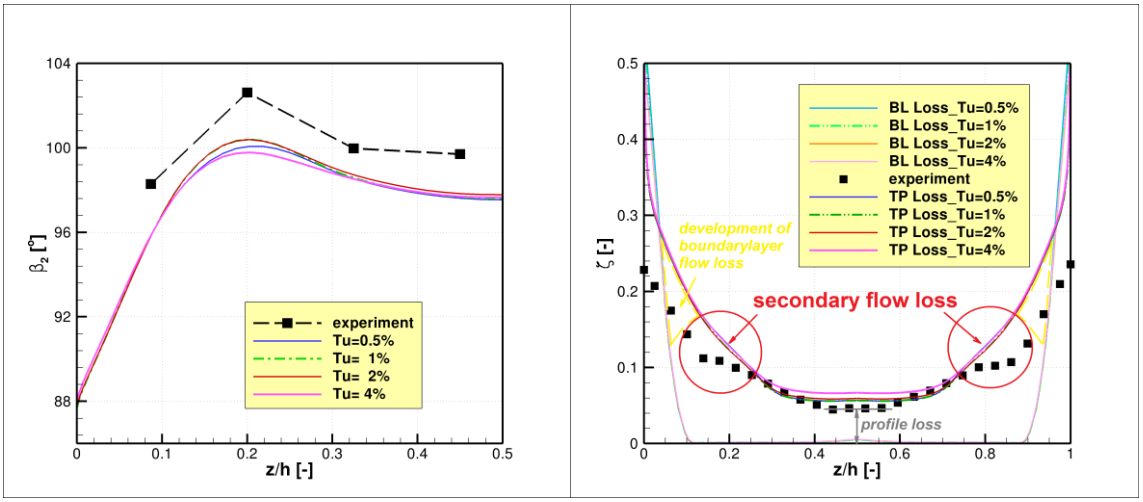

Fig.11 span-wise distribution of pitch-averaged outlet flow angle (left) and flow loss (right)

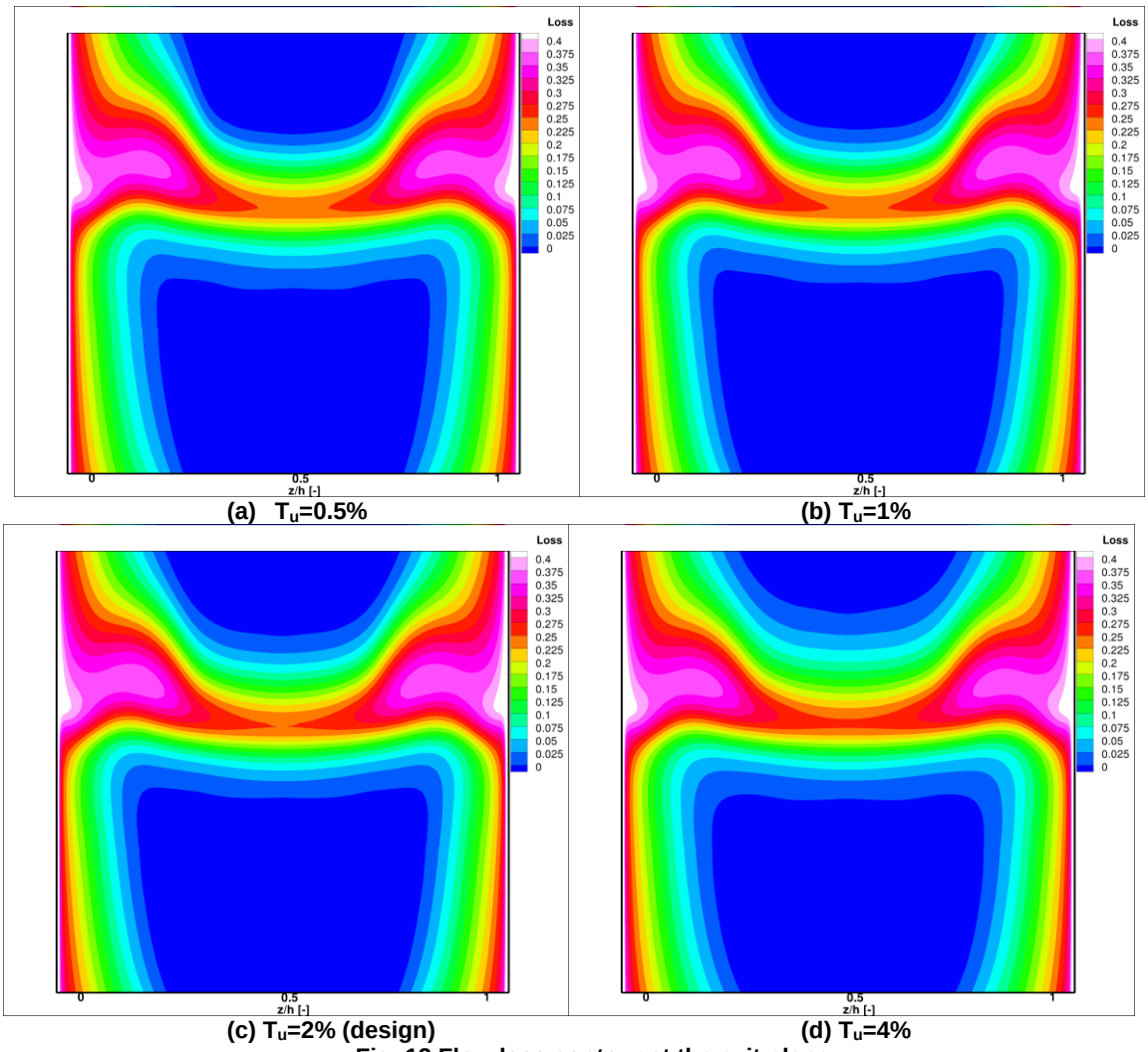

(a) T_u=0.5% (b) T_u=1%

(c) T_u=2% (design) (d) T_u=4%

Fig. 12 Flow loss contour at the exit plane

Figure 11 shows the span-wise distribution of pitch-averaged outlet flow angle and flow loss in the simulations validated by the experiment. The contours of total pressure loss coefficient at the exit plane are shown in figure 12. From figure 11 and 12, it can be found that, the inflow turbulence affects the outlet flow angles little, which are still of the similar trend as the experiment, but of slight differences on their amplitudes. The inlet boundary layer flow losses and its further development in the cascade are influenced little by the inflow turbulence variation, whilst the profile loss changed a lot. Additionally, the section of secondary flow loss has a very slight alteration due to the inflow turbulence variation. In our study, the secondary flow loss of case 4 (T_u=4%) has the same value as that of case 1(T_u=0.5%), while the case 3(T_u=2%) has the lowest secondary flow loss.

3) Suction-side wall shear stress and streamline

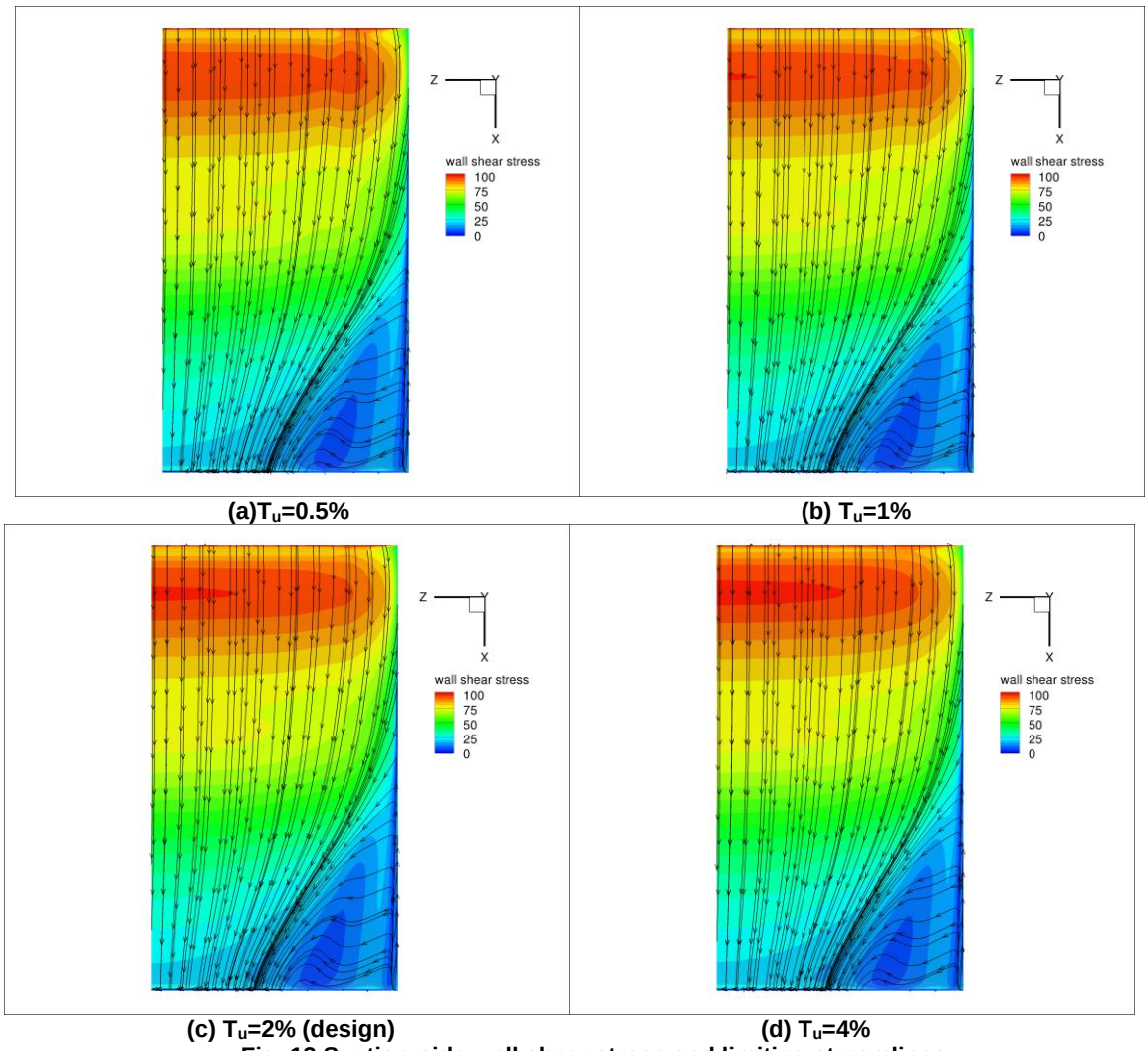

(a)T_u=0.5% **(b) T_u=1%**

(c) T_u=2% (design) **(d) T_u=4%**

Fig. 13 Suction-side wall shear stress and limiting streamlines

The higher inflow turbulence increases the disturbance of the profile boundary layer, so in figure 13, the suction-side wall shear stress of mainstream region from leading edge to 2/3 chord is improved with the increasing inflow turbulence, but has only slight effect on the corner vortex along the span-wise and axial direction.

4) Turbulent kinetic energy

The contours of turbulent kinetic energy in the cascade passage are shown in figure 14 with inflow turbulent intensity variation. Similarly as the figure 5(b), in these figures, the corner vortex trigger can be obviously found. Due to the suction side horseshoe vortex, the corner vortex can be found obviously at nearly 60% chord. Then one of the separations along suction side of the profile develops into the concentrated shed vortex, which can be recognized as the high turbulent kinetic energy area. The inlet turbulence influences the concentrated shed vortex a lot due to the decreasing area of the high turbulent kinetic energy with improved inflow turbulence.

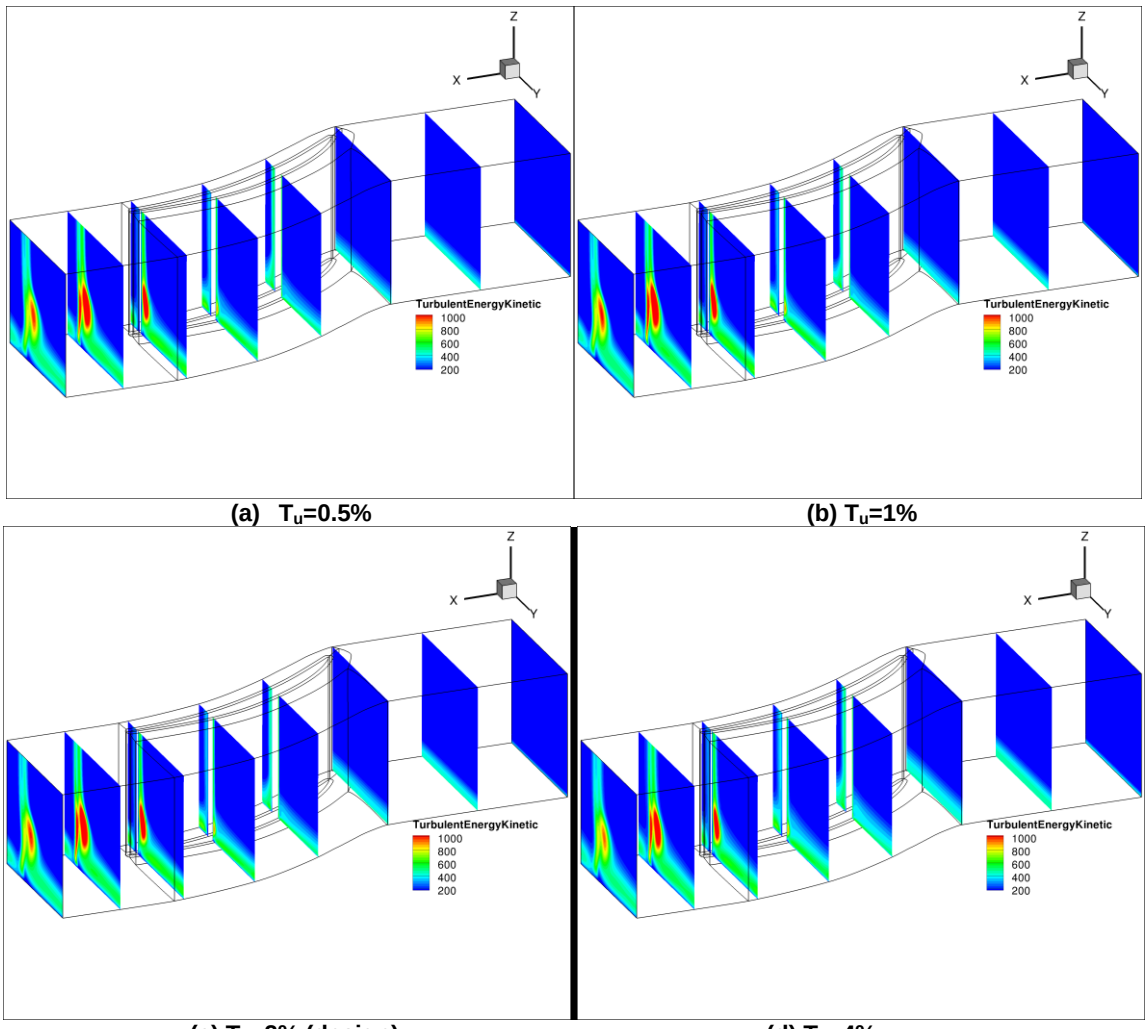

(a) T_u=0.5% (b) T_u=1%

(c) T_u=2% (design) (d) T_u=4%

Fig. 14 Turbulent Kinetic Energy

5) 3D streamline for wake vortex

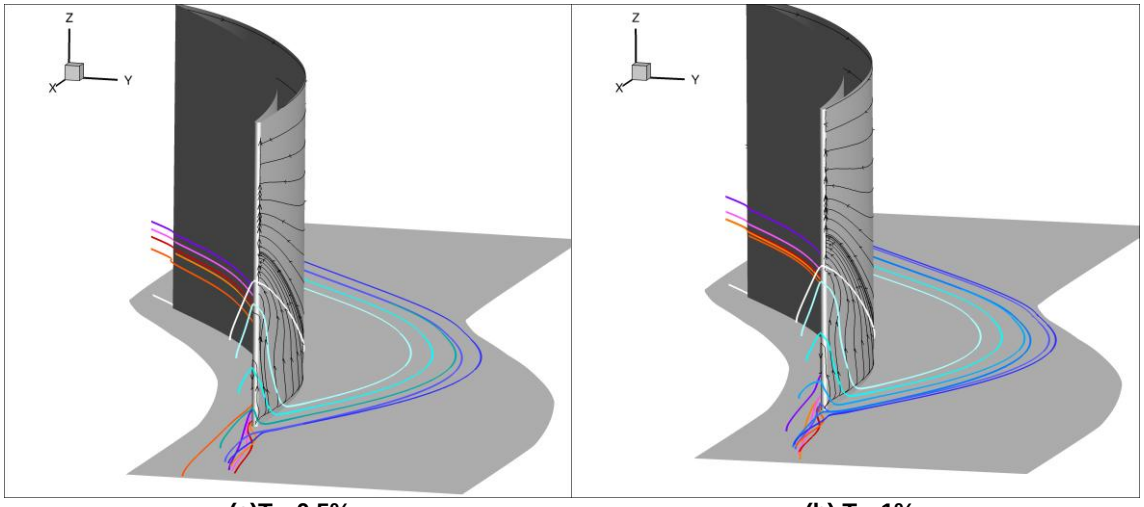

(a)T_u=0.5% (b) T_u=1%

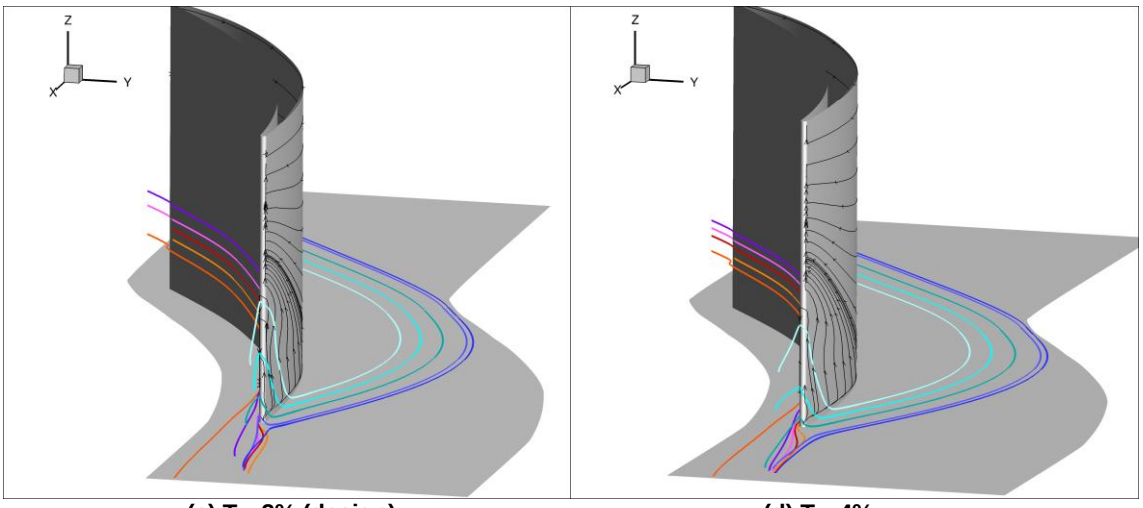

(c) T_u=2% (design) **(d) T_u=4%**

Fig. 15 3D streamlines of wake vortex

In figure 15, the 3D streamlines are shown to reveal the wake vortex. With different inflow turbulence, the wake vortex is somehow influenced. The flow coming through the pressure-side boundary layer goes down to the trailing edge near the hub-wall, where it interacts with the suction-side flow which coming from the inlet near the hub-wall. Then the two kinds of flow rotate together and swirl further to the downstream. However, when increasing the inflow turbulence, the wake vortex is similar to each case, but with less swirling vorticities.

CONCLUSIONS

In this paper, with the help of G3DMESH and the flow solver TRACE, we have showed and analyzed numerical simulations, of which the design case is highlighted with the validation of experimental results. The distribution of the total pressure loss is compared for simulation and experiment while the flow visualization is used for a general description of the flow topology in comparison with the numerical results. With the good agreement of the experimental validations, the results of numerical methods can be trusted in the throughout analysis in this paper.

The variation of inlet boundary layer thickness was performed at the design point of the blade (T_u=2%), δ_{99} ranging from 1mm to 5mm. The fully turbulent steady simulations are mainly concentrated on the influence of the inlet boundary layer thickness on the secondary flow and flow loss. With the analysis, it can be concluded that, 1) The inlet boundary layer thickness has a pronounced effect on the secondary flow behaviors and loss; 2) The inlet boundary layer thickness influences the side wall flow loss a lot, while the profile loss remains nearly constant; 3) The total pressure loss is affected by boundary layer thickness because of the changes of the corner vortex and concentrated shed vortex on the suction surface; 4) The inlet boundary layer thickness has a small influence on the variation of outflow angle, which is below 1 degree at the most; 5) However, the inlet boundary layer thickness changes three-dimensional distributions of flow loss at the exit; 6) With the analysis of iso-surface of axial vorticity, the horseshoe vortex on the suction side is in the corner region of the profile and the sidewall, but the pressure-side branch induced by the pressure gradient between the neighboring two cascades tends to develop in the passage and then becomes part of the passage vortex; 7) Due to the development of horseshoe vortex, the wall streamlines on the profile pressure-side on the leading edge and trailing edge show a slight displacement, while the suction side differs on the intensity and size of the corner separation/vortex along span-wise and axial direction; 8) Regarding the 3D streamlines in the

passage, when increasing the inlet boundary layer thickness, the passage vortex swirls much bigger, and the corner vortex is increased a lot to nearly half of the mid-span, while the wake vortex is similar to each case.

For the inflow turbulence variation, the simulations were based on the design inlet conditions with a designed boundary layer thickness. With the results of simulations, it can be concluded that 1) The inlet turbulence has a noticeable influence on the profile loss due to increased surface wall shear stress; 2) Its effect on the secondary flow behavior can be observed in the changes of the secondary flow loss at the exit plane; 3) Compared to the experiment, the inlet turbulence affects the exit flow angle little, which is still of the similar trend with the experiment along span. The maximum value of the exit flow angle is varied a little with the inlet turbulence variation; 4) The inlet turbulence alters the development of the sidewall boundary layer thickness, which can be obtained from the passage turbulent kinetic energy contours; 5) The analysis of the blade suction-side wall shear stress contours and the surface streamlines shows that the inlet turbulence increases the wall shear stress on the suction side, but has little effect on the corner separation/vortex along the span-wise and axial direction.

REFERENCES

[1] S. Farhan Ali Hashmi, Qiao, W. Y. and Chen, P. P., (2011): *Prediction of Hub Corner Stall Characteristics of a Highly Loaded Low Speed Single Stage Fan*, Journal of Thermal Science Vol.20, No.2 (2011), pp. 106-114.

[2] Chen, P. P., Qiao, W.Y., S. Farhan Ali Hashmi, Shi, P.J. and Zhao, L., (2011): *Passive control of hub-corner separation/stall using axisymmetric-hub contouring*, Proceedings of the Institution of Mechanical Engineers, Part G: Journal of Aerospace Engineering published online 21, December 2011, DOI: 10.1177/0954410011421716.

[3] Horlock, J. H. and Denton, J. D., (2005): *A review of some early design practice using computational fluid dynamics and a current perspective*, Journal of Turbomachinery, Vol.127(1):5-13.

[4] Horlock, J. H., Louis, J. F., Percival, P.M.E., Lakshminarayana B., (1966): *Wall Stall in Compressor Cascades*, Journal of Basic Engineering, Vol. 88(3):637-648.

[5] Choi, M., Park, J. and Baek, J., (2005): *EFFECTS OF THE INLET BOUNDARY LAYER THICKNESS ON THE FLOW AND LOSS CHARACTERISTICS IN AN AXIAL COMPRESSOR*, ASME Paper GT2005-68580.

[6] Wagner, J. H., Dring, R. P., and Joslyn, H. D., (1985): *Inlet Boundary Layer Effects in an Axial Compressor Rotor: Part I—Blade-to-Blade Effects*, Journal of Engineering of Gas Turbines Power, Vol. 107(2):374-380.

[7] Wagner, J. H., Dring, R. P., and Joslyn, H. D., (1985): *Inlet Boundary Layer Effects in an Axial Compressor Rotor: Part II—Throughflow Effects*, Journal of Engineering of Gas Turbines Power, Vol. 107(2):381-386.

[8] FENG, G. T., ZHANG, Y. J., CHEN, F. and SU, J. X., (2006)： *Influence of Inlet Boundary Layer on Flow Field Performance of the 2D Compressor Bowed Stator Vane (in Chinese)*, Journal of Aerospace Power, Vol. 21(2): 254-260.

[9] De Palma, P., (2006): *Numerical simulations of three-dimensional transitional compressible flows in turbomachinery cascades*, International Journal of Numerical Methods for Heat & Fluid Flow, Vol. 16(4): 509-529.

[10] Lei, V. M., Spakovszky, Z. S. and Greitzer, E. M., (2008): *A criterion for axial compressor hub-corner stall*, Journal of Turbomachinery, Vol. 130: 031006-1 – 031006-10.

[11] Sauer, H., Schmidt, R. and Vogeler, K., (2012): *Influence of Chord Length and Inlet Boundary Layer on the Secondary Losses of Turbine Blades*, Journal of Turbomachinery, Vol. 134: 011015-1 – 011015-9.

[12] Luo, H. L. (2009): *Numerical and Experimental Investigations on Aerodynamic Issues of Highly-Loaded Blading Design in Low-Pressure Turbine (in Chinese)*, Ph.D. Thesis, Northwestern Polytechnical University, Xi'an, China.

[13] Liesner, K. Meyer, R. (2008): "*Experimental setup for detailed secondary flow investigation by two-dimensional measurement of total pressure loss coefficients in compressor cascades*". VKI XIX Symposium on Measurement Techniques in Turbomachinery; Brussels, Belgium

[14] Weber, A. and Fox R., (2006): *TRACE v5.3*, DLR, Institute of Propulsion Technology, Cologne.

[15] Weber, A., (2008): *G3DMESH v4.5.4*, DLR, Institut fuer Antriebstechnik, Cologne.

[16] Liesner, K., Meyer, R., Lemke, M., Gmelin, C., Thiele, F., (2010): *ON THE EFFICIENCY OF SECONDARY FLOW SUCTION IN A COMPRESSOR CASCADE*, ASME Paper GT2010-22336